Diffusion in undoped and Cr-doped amorphous UO2

Owen, Megan; Cooper, Michael W D; Rushton, Michael; Claisse, Antoine; Lee, Bill; Middleburgh, Simon

Journal of Nuclear Materials

DOI:
10.1016/j.jnucmat.2023.154270

Published: 01/04/2023

Publisher's PDF, also known as Version of record

Journal of Nuclear Materials 576 (2023) 154270

Contents lists available at ScienceDirect

Journal of Nuclear Materials

journal homepage: www.elsevier.com/locate/jnucmat

Nuclear fuels and materials

Diffusion in undoped and Cr-doped amorphous UO_2

Megan W. Owen[a,*], Michael W.D. Cooper[b], Michael J.D. Rushton[a], Antoine Claisse[c], William E. Lee[a], Simon C. Middleburgh[a,*]

[a] Nuclear Futures Institute, School of Computer Science and Electronic Engineering, Bangor University, Bangor, Gwynedd, LL57 1UT
[b] Materials Science and Technology Division, Los Alamos National Laboratory P.O. Box 1663, Los Alamos, NM 87545, USA
[c] Westinghouse Electric Sweden AB, 721 63 Västerås, Sweden

ARTICLE INFO

Article history:
Received 26 September 2022
Revised 16 December 2022
Accepted 11 January 2023
Available online 13 January 2023

Keywords:
Amorphous
Grain boundaries
UO_2
Doped UO_2
Fuel manufacture

ABSTRACT

UO_2 fuel pellets are often doped with chromium oxide to obtain favourable properties such as higher density, improved thermal stability, large grain sizes, improved pellet-clad interaction margins, and increased fission gas retention during transients. Chromium has a low solubility limit in UO_2, with past experimental work reporting solubility limits ranging between 0.004 to 0.06 wt.% Cr. Due to its low solubility, segregation of Cr ions to the grain boundary may occur. Further, the complexity of these boundaries may be high as observed in other ceramics resulting in disordered or amorphous regions along the boundary, affecting a range of material and operational properties of the fuel pellet. To assess these disordered regions, in this work we study amorphous undoped and Cr doped UO_2 systems (containing 10–50 at.% Cr^{3+}) that have been modelled using classical molecular dynamics methods incorporating Cr^{3+} into the well-used CRG potential library. Diffusion coefficients, pre-exponential factors, and activation energies for diffusion were computed for oxygen ions, assessing the impact of structure and extrinsic species on migration. Oxygen diffusion was observed to be much faster in the undoped amorphous system compared to its crystalline counterpart. Oxygen diffusion in doped systems decreased with increasing Cr concentration, highlighting the importance of additives to retain fission products and other migratory species.

1. Introduction

Doped UO_2 fuel pellets are being considered for widespread use in commercial light water reactors due to their expected enhanced performance and benefits with respect to pellet manufacture. Oxides with low solubilities in UO_2, such as SiO_2, Al_2O_3 Cr_2O_3 or Al_2O_3 + Cr_2O_3, have been observed to enhance grain growth and densification during fabrication, even when added in small amounts (ranging from a few hundred to a thousand parts per million by weight – wppm). This leads to some favourable properties such as higher density, reductions in fission gas release during transients, improved pellet-clad interaction margins, improved resistance against post failure degradation, and improved corrosion resistance [1,2].

Experimental and theoretical work on grain boundaries in UO_2 by Nerikar et al. [3], has shown that most grain boundaries in UO_2 are not classified as coincident site lattice (CSL) boundaries, only approximately 16% of grain boundaries were classified as such. Bourasseau et al. [4] also found that CSL grain boundaries represent between 15 – 20% of linear grain boundaries observed in polycrystalline UO_2, with most grain boundaries being non-CSL. Insoluble dopants, fission products or impurities are often found to segregate towards grain boundaries [5]. Theoretical work by Hong et al. [6] shows that aliovalent fission products segregate to grain boundaries in UO_2. Dopants or impurities segregating towards the open grain boundaries, may induce further amorphization/increases in complexity [7], or in the case of insoluble fission gases, form bubbles [8]. Cr has also been observed to form solid precipitates at grain boundaries, included as a separate phase to the UO_2 matrix due to its low solubility as approximately 1500 ppm [9]. Symington et al. [10] modelled UO_2 grain boundaries using molecular dynamics simulations, showing that structural changes were observed as a function of temperature for both coincident site lattice boundaries, $\Sigma5(210)$ and $\Sigma5(310)$, facilitated by the presence of impurities. Similar structural changes may be affecting the grain boundary properties in doped UO_2 fuel. Grain boundary properties are important for a number of phenomena that impact fuel performance in-reactor. For example, vacancy diffusion along grain boundaries is the primary mechanism by which intergranular bubbles swell and interconnect leading to fission gas

* Corresponding authors.
E-mail addresses: megan.owen@bangor.ac.uk (M.W. Owen), s.middleburgh@bangor.ac.uk (S.C. Middleburgh).

https://doi.org/10.1016/j.jnucmat.2023.154270

release [11]. Similarly, self-diffusion at grain boundaries under irradiation controls Coble creep.

Assmann et al. [12] found experimentally that Nb_2O_5 doped UO_2 increased fission gas retention due to the decrease of fission product migration (Cs, I), alongside increasing grain growth. Experimental work conducted by Costa *et al.* [13] also agrees with these positive findings for Nb_2O_5 doped UO_2, with increased grain sizes and density reported in comparison to undoped UO_2. Irradiation does not seem to affect large grain sizes formed in doped UO_2 systems, shown by experimental work conducted by Killeen [14]. Different concentrations of Nb_2O_5 and La_2O_3 were added to UO_2 systems, and were subjected to six cycles of irradiation, at temperatures varying between 1423 and 1537 °C. Results here found grains of 28 μm and 80 μm in unannealed, and annealed, 1.0 mol.% Nb_2O_5 doped UO_2, respectively, were stable under irradiation.

Contrasting conclusions are reported in literature regarding diffusion along and across grain boundaries of UO_2. Theoretical work by Williams et al. [15] has found that oxygen diffusion is enhanced at grain boundaries, dependant on the temperature and local structure of the boundary. Oxygen and uranium self-diffusion in doped UO_2 has been reported to increase in the presence of dopants and impurities. Doping with trivalent dopants such as La_2O_3 creates oxygen vacancies for charge balancing purposes, increasing the rate of oxygen diffusion [10,16]. Uranium diffusion has been observed to increase in the presence of pentavalent dopants such as Nb_2O_5 due to the increase in population of uranium vacancies [16]. The self-diffusion of oxygen and uranium species is observed to be faster of that observed for defects, such as fission gas products [16]. Such phenomena may be responsible for enhancing concentrations of defects at the grain boundary regions in UO_2. However, experimental work by Sabioni et al. [17] reveals that grain boundaries do not contribute to greater oxygen diffusion, rather, that grain boundaries have a greater effect on uranium diffusion. Grain boundaries in oxides such as UO_2 have also been reported to block ionic transport across the boundary due to a space charge effect, arising when segregation of charged defects to the boundary decreases ionic mobility across the boundary [10]. Kubo et al. [18] found from experimental work, that Gd dopants were found to segregate to grain boundary regions in UO_2 fuel, forming a doped grain boundary of thickness between 1 – 3 nm, increasing with increasing Gd concentration. The conductivity was found to decrease with increasing Gd additions. This was due to an increase in the electric potential barrier formed along the grain boundary, hindering electron-hole migration in this region.

This work aims to analyse amorphous undoped and Cr doped systems, to observe the impact of the dopants on potentially disordered grain boundary (amorphous) regions using theoretical methods based upon molecular dynamics. The diffusion of oxygen ions was analysed between 500 – 900 K for all systems, to observe whether increasing dopant concentration impacts diffusion, and whether the initial structure type dictates diffusion events. Analysis of diffusion in these systems will enable a better understanding of diffusivity and mechanisms of diffusion along grain boundary regions in undoped and doped UO_2.

2. Methods

2.1. Potential fitting

A Cr_2O_3 potential has been developed in this work in a way that enables its use in combination with the Cooper, Rushton, Grimes (CRG) actinide oxide potentials [19]. In line with the CRG potential, Cr^{3+} is treated as having partial charge of 1.6656e (where e is the elementary charge), which is proportional to its formal charge based on an ionicity of 0.5552. Potential fitting has been carried out using available experimental data for Cr_2O_3. The potential form has been kept consistent with that used by CRG [19] to enable the application of this potential to Cr_2O_3 -doped UO_2 and other doped or mixed oxide systems. Therefore, in addition to using the same value of ionicity for the Cr^{3+} ions, the O^{2-} - O^{2-} parameters are fixed at the values derived previously for actinide oxides [19]. Cr^{3+} - O^{2-} pairwise interactions include Coulombic (ϕ_C), Morse (ϕ_M), Buckingham terms (ϕ_B), while Cr^{3+}-Cr^{3+} interactions include just Coulombic and Buckingham terms. Embedded atom method (EAM) parameters have been included for Cr^{3+} using the same potential form as for the original CRG model. The Morse, Buckingham, and EAM parameters were optimized using the Potential-Pro-Fit (PProFit) fitting software [20]. The energy of a given atom i in the system is described as a sum over the other atoms in the system j:

$$E_i = \frac{1}{2}\sum_j \phi_{\alpha\beta}(r_{ij}) - G_\alpha \sqrt{\sum_j \sigma_\beta(r_{ij})}$$

where α and β are the species of atoms i and j, and r_{ij} is the separation between i and j. $\phi_{\alpha\beta}$ describes the pairwise interactions as follows:

$$\phi_{\alpha\beta}(r_{ij}) = \phi_C(r_{ij}) + \phi_B(r_{ij}) + \phi_M(r_{ij})$$

$$\phi_C(r_{ij}) = \frac{q_\alpha q_\beta}{4\pi\epsilon_0 r_{ij}}$$

$$\phi_M(r_{ij}) = D_{\alpha\beta}\left[\exp(-2\gamma_{\alpha\beta}(r_{ij} - r_{\alpha\beta}) - 2\exp(-\gamma_{\alpha\beta}(r_{ij} - r_{\alpha\beta})\right]$$

$$\phi_B(r_{ij}) = A_{\alpha\beta} exp\left(\frac{-r_{ij}}{\rho_{\alpha\beta}}\right) - \frac{C_{\alpha\beta}}{r_{ij}^6}$$

where q_α and q_α are the ionic charges, as already described, and $D_{\alpha\beta}$, $\gamma_{\alpha\beta}$, $r_{\alpha\beta}$, $A_{\alpha\beta}$, $\rho_{\alpha\beta}$, $C_{\alpha\beta}$ are the pair parameters optimized during fitting. To prevent unphysical short-range interactions, ZBL potentials were splined to the short range pairwise components, as described in more detail later. The many body interactions are described by $-G_\alpha\sqrt{\sum_j \sigma_\beta(r_{ij})}$, whereby the embedding function is of square root form (with the coefficient $-G_\alpha$) applied to a sum of functions (σ_β) representing the electronic density contribution from the surrounding atom j at the position of atom i. $\sigma_\beta(r_{ij})$ is described by:

$$\sigma_\beta(r_{ij}) = \left(\frac{n_\beta}{r_{ij}^8}\right)\frac{1}{2}\left(1 + erf\left(20(r_{ij} - 1.5)\right)\right)$$

where erf is an error function applied so that the EAM contribution to the potential is cut-off smoothly below 1.5 Å, which prevents unphysical forces occurring at short separations. G_α and n_β are empirical parameters optimized during fitting.

For a given candidate parameter set, the 300 K lattice parameters were calculated using MD simulations in Large-Scale Atomic/Molecular Massively Parallel Simulator (LAMMPS) that employ a Nose-Hoover thermo and barostat with relaxation times of 0.04 ps and 0.1 ps, respectively, within an NPT ensemble at zero pressure. A timestep of 2 fs was used. The 0 K elastic constants for the candidate parameter set were determined using the General Utility Lattice Program (GULP) [21]. A merit function was then constructed based on the difference in the predicted lattice parameters and single crystal elastic constants compared to the experimental values from Hill et al. [22], and Alberts and Boeyan [23], respectively. The parameters were then optimized by minimizing the merit function using a Nelder-Mead algorithm [24] to ensure a good match to the experimental data.

Validation of the final parameter set was carried out against the temperature dependence of the a and c lattice parameters of

Table 1
Number of atoms per species for UO_2 systems.

System	Species			Total
	U	O	Cr	
UO_2	2048	4096	–	6144
10 at.% Cr doped UO_2	1844	3994	204	6042
20 at.% Cr doped UO_2	1683	3891	410	5939
30 at.% Cr doped UO_2	1434	3789	614	5837
40 at.% Cr doped UO_2	1228	3686	820	5734
50 at.% Cr doped UO_2	1024	3584	1024	5632

Cr_2O_3, as measured by Dymshits et al. [25] and Kudielka [26]. For validation, a 4 × 4 × 2 extension of a corundum unit cell was selected and the same thermostat, barostat, and timestep as used in the fitted procedure were employed. The lattice parameters were evaluated from 250 K to 2000 K at 25 K intervals by equilibrating the system for 15 ps, followed by sampling and averaging over another 15 ps.

2.2. Structure generation

Atomsk [27] was used to generate an 8 × 8 × 8 supercell of the fluorite polymorph of UO_2. Using the undoped system, Cr concentrations between 10 at.% and 50 at.% were analysed, by substituting chromium randomly for uranium, to sample a number of configurations. Upon introducing Cr into the system, oxygen vacancies were applied to preserve charge neutrality. As Cr^{3+} is of a lesser charge state than U^{4+}, one oxygen vacancy was generated for every two Cr ions substituted (akin to the crystalline system [28]). Ten different structures were generated using Atomsk for each system considered in this work, to sample a broad range of configurations.

The number of atoms per concentration is shown in Table 1. These values were chosen to identify the general behaviour of species in the absence and presence of Cr dopants, not necessarily mimicking the concentrations expected in doped fuel, particularly the bulk UO_2 concentration that is typically ~1000 wppm. Saying this, the local concentration at grain boundaries is expected to be higher, as found in Gd doped UO_2, where Gd ions segregated towards grain boundaries, increasing the concentration at the grain boundary, relative to the bulk [18]. Chromium is reported to have an extremely low solubility in UO_2, with experimental work conducted by Leenaers et al. [29] reporting the solubility limit for Cr in UO_2 at sintering temperatures of 1600 °C, 1660 °C, and 1760 °C, as 0.065, 0.086, and 0.004 wt.% Cr, respectively. Crystalline Cr doped systems are therefore not reported here as they are expected to be unrealistic systems to model. Past work considered the accommodation of Cr^{3+} into UO_{2+x} where the Cr was accommodated by U^{5+} cations [28], and although not considered in this work, the potential implications are discussed.

To generate the amorphous systems, a melt-quench procedure was conducted using classical molecular dynamics (MD) within the LAMMPS program [30]. The UO_2 systems were described using a many-body potential from the Cooper-Rushton-Grimes (CRG) model [19], which accurately describes the U^{4+} - O^{2-} system. This potential has proven efficient in describing both crystalline and amorphous UO_2 [19]. All crystalline starting structures were heated from 300 K to 5000 K in 100 ps under an isothermal-isobaric (NPT) ensemble, to fully melt the crystalline structure. The systems were held at 5000 K under an NPT ensemble for a further 100 ps to ensure the systems were fully melted. The systems were then ramped down in temperature in 100 K increments under an NPT ensemble, ramping down in temperature over 20 ps, before being held at the target temperature for a further 20 ps. Quenching from 5000 K to 300 K took a total of 1880 ps, as shown in Fig. 1. Upon reaching 300 K, the systems were held for a further 100 ps under an NPT ensemble for equilibration purposes.

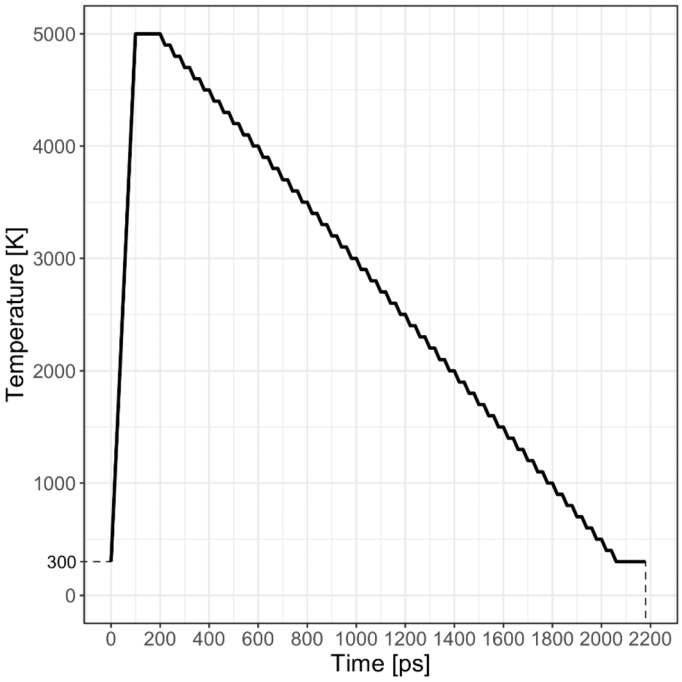

Fig. 1. Molecular dynamics melt-quench procedure.

Densities of the undoped and Cr doped UO_2 systems were calculated using MD. For the 10 structures for each system, the structures were equilibrated at 300 K for 50 ps, over which the density was calculated. The values of density for the 10 structures over this period were then averaged to give the values found herein.

2.3. Diffusion in UO_2

Using the ten different structures for the amorphous systems generated in Section 2.2., MD calculations were conducted to analyse diffusivity of the constituent ions. The systems were initially equilibrated at 300 K for 30 ps, before being heated from 300 K to the temperatures of interest (500 – 900 K) in 100 K increments under an NPT ensemble. This temperature range was chosen as the crystallisation temperature of amorphous UO_2 is reported experimentally as 948.15 K [31], therefore analysis of temperatures above this would be unfeasible for the undoped system. This experimental work by Matzke et al. [31] was performed in un-irradiated conditions on thin film UO_2, which can be related amorphous grain boundary phases as they have previously been described as intergranular films [7]. Each 100 K increment was conducted by ramping the system up in temperature over 10 ps, before holding at temperature for a further 10 ps. Upon reaching the temperature of interest, the systems were held for a further 10 ps under an NPT ensemble, before switching to an NVT ensemble and holding the system for a further 10 ps. Mean squared displacement (MSD) calculations were conducted over 20 ns for all constituent ions. The MSD was plotted against time, allowing the diffusion coefficients to be calculated over the equilibrated portions of the plots. The MSD calculated using Eq. (1) is based on random walk theory in 3D, which has been used successfully in previous works on oxygen diffusion in crystalline and amorphous ZrO_2 [32].

$$\mathrm{MSD} = 6\mathrm{D}t + B \tag{1}$$

Where D is the diffusion coefficient (cm^2/s), t is the time (s), and B is the thermal vibration of the ions about their position in the structure.

Arrhenius behaviour has been assumed for all systems, allowing the data to be fit to Eq. (2), where D_o is the pre-exponential factor

Table 2
The Cr^{3+}-O^{2-} and Cr^{3+}-Cr^{3+} pairwise parameters derived in this work and the O^{2-}- O^{2-} pairwise parameters fixed at values originally derived by CRG for actinide oxides [19].

Pairwise parameter	Cr^{3+}-O^{2-}	Cr^{3+}-Cr^{3+}	Cr^{3+}-U^{4+}	O^{2-} -O^{2-} [16]
$A_{\alpha\beta}$ (eV)	1156.49	2695.52	10,647.76	830.28
$\rho_{\alpha\beta}$ (Å)	0.2795	0.1179	0.1800	0.3529
$C_{\alpha\beta}$ (eVÅ^6)	0.0	0.0	0.0	3.884
$D_{\alpha\beta}$ (eV)	1.348	–	–	–
$\gamma_{\alpha\beta}$ (Å^{-1})	2.245	–	–	–
$r_{\alpha\beta}$ (Å)	1.799	–	–	–

Table 3
The empirical potential Cr^{3+} many-body parameters derived in this work and the O^{2-} values fixed at the values originally derived by CRG for actinide oxides [19].

Coulomb and EAM parameters	Cr^{3+}	O^{2-}
q_α (e)	1.6656	−1.1104
G_α (eVÅ$^{1.5}$)	1.517	0.690
n_β (Å^5)	0.0	106.85

for diffusion (cm^2/s), Q_d is the activation energy for diffusion (eV), R is the gas constant, equivalent to the Boltzmann constant (8.63 × 10^{-5} eV/K/atom), and T is the temperature (K).

$$D = D_o \exp\left(\frac{-Q_d}{RT}\right) \quad (2)$$

The Van Hove auto-correlation function can be used to analyse the mechanism of diffusion within amorphous systems. The function is a probabilistic function, separated into distinct and self-parts [33]. The self-part (G_s) is considered in this work, which calculates the probability density of finding a particle, i, at a time, t, given that the same particle was at the origin at $t = 0$ [33]. This function has been applied to trajectories of oxygen, uranium, and chromium diffusion at 500 K and 900 K in the undoped and doped systems, to analyse the mechanism of diffusion within these disordered systems.

3. Results

3.1. Cr^{3+} potential fitting

Tables 2 and 3 show the final parameter set for the Cr_2O_3 potential. As discussed previously, the same potential form as for the UO_2 interactions were used for Cr_2O_3, which include Coulomb, Morse, Buckingham, and EAM terms. The cation-cation pairwise interactions (Cr^{3+} - Cr^{3+}, Cr^{3+} - U^{4+}) used only Coulomb and Buckingham terms, whereas Cr^{3+} - O^{2-} also includes a Morse term (see Table 2). The O^{2-} - O^{2-} potential parameters were fixed based on the original version of the CRG potential [19]. For both Cr^{3+} and O^{2-}, an EAM potential was used to introduce many-body effects and, while the Cr^{3+} parameters have been optimized here, the O parameters were fixed based on the CRG potential [19] (see Table 2). The ionic charges were not optimized but were scaled proportionally to the formal charges, such that partial charges of 1.6656e and −1.1104e were used to represent Cr^{3+} and O^{2-}, respectively. To enable use of the potential for Cr-doped UO_{2+x}, Cr^{3+}-U^{4+} and Cr^{3+}-U^{5+} interactions were included and are based only on Coulombic and Buckingham interactions, where the latter were not fitted but instead are assigned based on the following equations:

$$A_{\alpha\beta} = \frac{1}{2}(A_{\alpha\alpha} + A_{\beta\beta})$$

$$\rho_{\alpha\beta} = (\rho_{\alpha\alpha} + \rho_{\beta\beta})^{\frac{1}{2}}$$

Table 4
A summary of the experimental data for crystallographic information [13] and elastic constants [23] used to fit the potential, alongside the values given by the final potential. MD at 300 K was used to determine the lattice parameters (a, b, c, α, β and γ), while energy minimization static calculations were used for the elastic constants (C_{11}, C_{12}, C_{13}, C_{14}, C_{33}, and C_{44}).

Property	Expt. [19,20]	Potential
$a = b$ (Å)	4.957	4.955
c (Å)	13.592	13.589
$\alpha = \beta$ (°)	120	120
γ (°)	90	90
C_{11} (GPa)	374	425.0
C_{12} (GPa)	148	200.4
C_{13} (GPa)	175	194.0
C_{14} (GPa)	−19	2.3
C_{33} (GPa)	362	391.4
C_{44} (GPa	159	131.3

where $A_{\alpha\beta}$ and $\rho_{\alpha\beta}$ are the mixed cation Buckingham interaction parameters and $A_{\alpha\alpha}$, $A_{\beta\beta}$, $\rho_{\alpha\alpha}$, and $\rho_{\beta\beta}$ are those for like-pairs of cations. A similar approach was used for mixed actinide oxide systems using the same potential [34].

ZBL potentials (describing screened nuclear coulombic repulsion) were splined to the short-range pair potentials to ensure that unphysical forces do not occur at very small separations, where the fitted potentials are not designed to be accurate. The cut offs for the splines were selected to ensure a smooth transition between the fitted pair interactions and the ZBL potentials. For O^{2-}-O^{2-}, Cr^{3+}-O^{2-}, U^{5+}-O^{2-}, U^{4+}-O^{2-}, Cr^{3+}-Cr^{3+}, U^{5+}-U^{5+}, U^{4+}-U^{4+}, and U^{4+}-U^{5+}, the short-range and long-range spline cut offs are 0.8 Å and 1.5 Å, respectively. For Cr^{3+}-U^{4+} and Cr^{3+}-U^{5+}, the short-range and long-range spline cut offs are 0.8 Å and 2.4 Å, respectively.

The lattice parameters and elastic constants given by the final model are reported in Table 4, alongside the experimental reference data. It can be seen that an excellent match to the lattice parameters has been achieved. Although there is a significant error for some of the elastic constants, the general trends are reproduced. The inability to reproduce the elastic constants exactly was likely due to the restriction that the O^{2-} - O^{2-} parameters must remain fixed at those derived for the original CRG potential, which was necessary to ensure the new potential could be applied to Cr doped oxides or Cr_2O_3 interfaces with other oxides already included in the CRG potential set.

Validation of the new model was carried out by simulating the lattice parameter for Cr_2O_3 as a function of temperature and comparing to the experimental data of Dymshits et al. [25] and Kudielka [26]. This data was not used in the development of the potential and, thus, enables the predictive capabilities of the potential to be tested and validated. Fig. 2 shows the experimental data alongside the prediction. An excellent agreement is obtained with the Dymshits data, whereby the new potential model captures the lattice parameter accurately over a wide range of temperatures and is within the noise of the experimental data. The empirical potential only slightly over-predicts the lattice parameter compared to the high temperature data from Kudielka *et al.* [26]. At the highest temperature data point from Kudielka [26] (at 1943 K) the percentage errors for a and c are 0.02% and 0.17%, respectively, representing an excellent agreement. Given that the thermal expansion was not included in fitting Fig. 2 demonstrates the predictive capabilities of the potential.

3.2. Amorphous UO_2 structures

3.2.1. Undoped UO_2

Amorphous undoped UO_2 systems were generated successfully. Radial distribution functions (RDF) and partial radial distribution functions were generated for each system at 300 K to analyse the

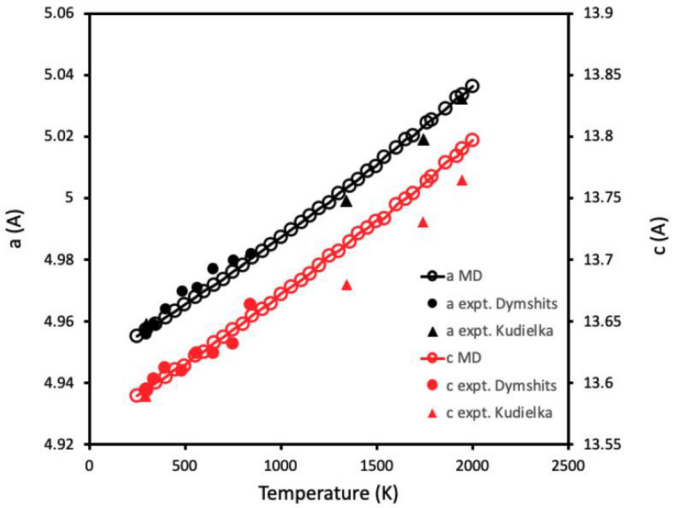

Fig. 2. MD simulations of the a and c lattice parameters of Cr_2O_3 as a function of T. Experimental data from Dymshits et al. [25] and Kudielka [26] are shown for validation.

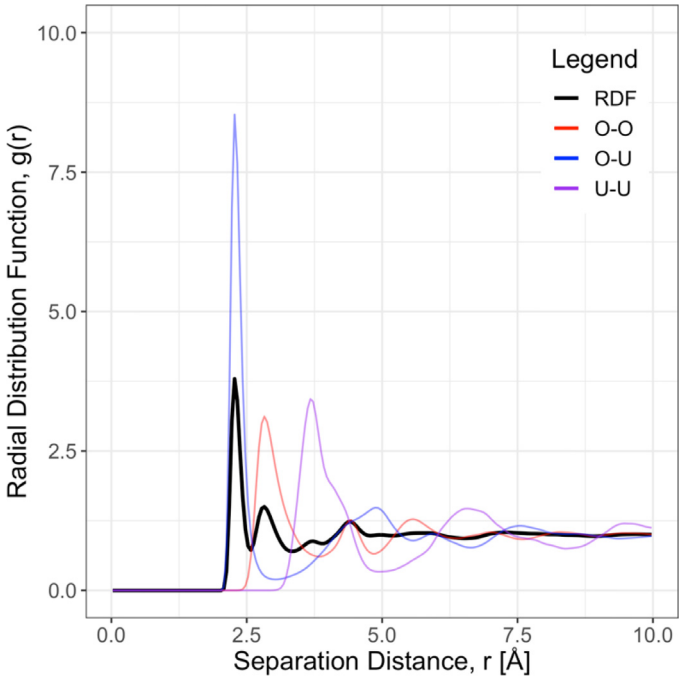

Fig. 3. Radial distribution function and partial radial distribution functions for amorphous undoped UO_2 at 300 K.

structures formed. Fig. 3 shows the radial distribution function and partial radial distribution functions for the amorphous undoped UO_2 systems.

The radial distribution function and partial radial distribution functions for the amorphous system have two characteristic peaks before oscillating around a value of g(r) = 1, indicative of an amorphous system. The two peaks for the radial distribution function are located at 2.28 Å and 2.83 Å, whereby the two peaks for the O - O, O - U, and U - U pairs are located at 2.83 Å and 4.43 Å, 2.28 Å and 4.88 Å, and 3.68 Å and 6.58 Å, respectively. The location of these peaks relates well with previous literature, whereby Middleburgh et al. used classical molecular dynamics to generate amorphous UO_2 [1].

A 5 Å slice along the (011) plane in undoped amorphous UO_2 is shown in Fig. 4, highlighting the amorphous network formed. The

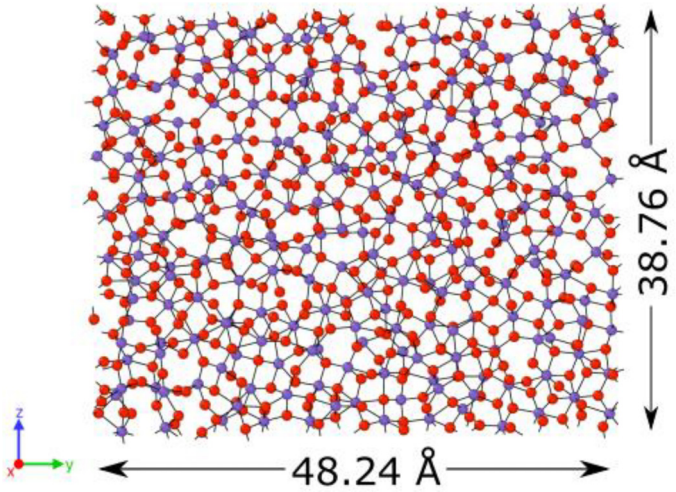

Fig. 4. 5 Å slice along the 011 plane through undoped amorphous UO_2 at 300 K, where oxygen = red, uranium = purple, U-O bonds = black.

coordination environment has been analysed for O - U and U - O pairs. On average, oxygen ions are coordinated with 3.65 uranium ions, whereas uranium ions are coordinated with 7.31 oxygen ions. The coordination numbers for the amorphous systems are very similar to that found in the crystalline UO_2 system, where oxygen ions are coordinated with 4 uranium ions, and uranium ions are coordinated with 8 oxygen ions as noted previously [1]. The decrease in coordination number noted for the amorphous system simulated here is due to the lack of the presence of a lattice. Opposite to crystalline systems, amorphous systems do not have specific lattice sites which atoms occupy; therefore, the coordination number of ions will vary throughout the structure. Fig. 4 highlights this further, as oxygen and uranium ions occupy random space within the system.

The density of the undoped amorphous UO_2 systems were calculated successfully, with an averaged value given as 10.55 g/cm^3. This is less than the experimental value observed for the crystalline counterpart of 10.97 g/cm^3 [35]. However, the decreased value relates well with other modelling works on undoped amorphous UO_2, showing that amorphisation may lead to an increase volume of the system [1].

3.2.2. Doped UO_2

Amorphous Cr doped UO_2 systems were generated successfully. Radial distribution functions and partial radial distribution functions for the doped systems were also analysed. Fig. 5 shows the radial distribution function for the amorphous Cr-doped systems at all concentrations. With increasing concentrations of Cr, the prevalence of the first peak at 2.03 Å becomes more prominent, with the prevalence of the second peak at 2.23 Å diminishing. The first peak here represents the Cr–O pair, with the second peak representing the U–O pair. These changes can be attributed to the increasing concentrations of Cr^{3+} - O^{2-} in the system in comparison to UO_2. This is a similar Cr^{3+} - O^{2-} bond distance predicted by Carey and Nolan [36] in their computational work on Cr_2O_3, where bond lengths for Cr – O were found to range between 2.02 Å and 2.05 Å. The third peak at 3.23 Å is relatively unaffected, with a slight decrease in intensity associated with a reduction in the overall U-U values.

A 5 Å slice along the (011) plane was taken for the 10 at.% and 50 at.% Cr doped amorphous doped UO_2 systems. The coordination environment has been analysed for the O-U, U-O,

O–Cr, and Cr-O pairs. All values have been time averaged. For the 10 at.% Cr doped systems, oxygen ions are coordinated

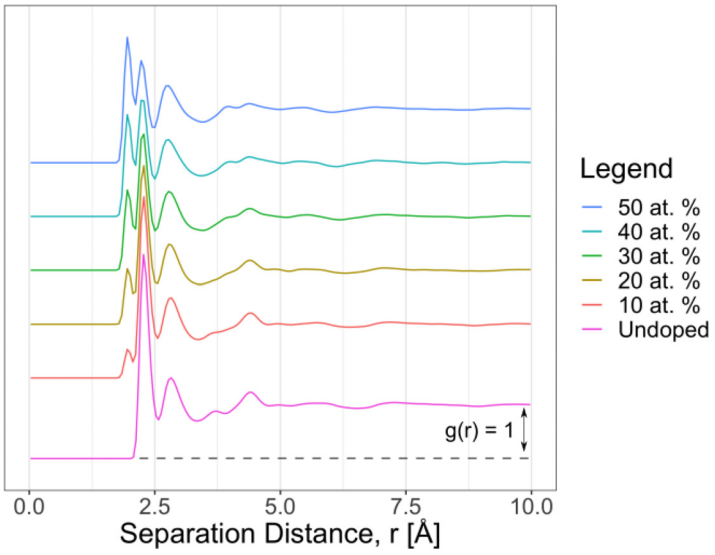

Fig. 5. Radial distribution functions for amorphous UO_2 systems at 300 K.

with 3.40 uranium ions, uranium ions are coordinated with 7.37 oxygen ions, chromium ions are coordinated with 5.84 oxygen ions, and oxygen ions are coordinated with 0.30 chromium ions. For the 50 at.% Cr doped systems, oxygen ions are coordinated with 2.14 uranium ions, uranium ions are coordinated with 7.50 oxygen ions, chromium ions are coordinated with 5.85 oxygen ions, and oxygen ions are coordinated with 1.67 chromium ions.

With increasing concentration of Cr, the coordination number of O - U pairs decreases, whereas the U – O coordination number increases. This is reasonable due to the fewer number of U ions in the system, due to substitutional Cr dopants. Due to the change in the host matrix, the increase in U – O coordination number is also reasonable. Similar effects have been observed in cubic ZrO_2 [37] and can be related to the results observed in the amorphous system here. The introduction of undersized trivalent dopants in cubic ZrO_2 was reported to leave dopant cations in a six-fold coordination with oxygen ions, alongside sharing an oxygen vacancy [37]. This enables the host cation (U in this case) to be associated with oxygen ions in the system, retaining or increasing its coordination number. However, the coordination of Cr - O has stayed relatively similar, whereas the O – Cr coordination number has increased. This relates well with the increasing numbers of Cr ions in the system.

In comparison to the undoped amorphous UO_2 system, the coordination number of O - U has decreased for both doped systems, whereas the coordination number of U – O has increased or stayed relatively similar to that observed in the amorphous undoped system. Cr ions are acting to maintain the original amorphous UO_2 network, however, they act as network modifiers in this instance due to the presence of non-bridging oxygens throughout, as observed in Fig. 6. [1,38].

The densities of the Cr doped UO_2 systems were calculated successfully, as shown in Table 5. With increasing Cr concentration, the density of the system decreases. As oxygen vacancies are generated for charge balancing purposes, fewer atoms are found in the system, and the mass of Cr is considerably smaller than U that it is replacing. As Cr segregation to the grain boundary may induce a disordered region, this will differ (in terms of atomic packing) substantially to that found in the bulk. The lower densities with increased Cr concentration therefore relates well with that hypothesised here, that increased Cr concentration induces disorder, and therefore decreases the density of the system.

Table 5
Densities of amorphous Cr doped UO_2 at 300 K.

Cr Concentration [at.%]	Density [g/cm^3]
10	10.27
20	9.94
30	9.59
40	9.17
50	8.70

3.3. Diffusion in amorphous UO_2

Diffusion in amorphous undoped UO_2 has been computed successfully. Oxygen diffusion in amorphous undoped UO_2 was observed to be much faster than that observed for uranium diffusion, with uranium ions being mostly immobile over the temperature range simulated. Fig. 6 shows the Arrhenius plot for oxygen diffusion in amorphous undoped UO_2.

From the Arrhenius plot, the activation energy and pre-exponential factors for oxygen diffusion were calculated as 0.30 eV $\pm$ 0.05 and 3.32 $\times$ 10^{-8} cm^2/s ($+$ 4.28 $\times$ 10^{-8}, - 1.87 $\times$ 10^{-8}), respectively. Only one activation energy was calculated for the temperature range here, as the calculations were being conducted on amorphous systems which were unaffected in terms of structure in the temperature range simulated. The error bars included in Fig. 7 consider the standard error of the simulation runs considered for undoped UO_2. In comparison to crystalline undoped UO_2 systems, the activation energies reported here for oxygen diffusion is much lower, indicating that diffusion in amorphous undoped systems is much faster than that observed for crystalline undoped systems.

A review by Murch et al. [38] reported the activation energy for oxygen diffusion mediated by a vacancy mechanism in stoichiometric UO_2 as 0.52 eV, much higher than that reported here. For uranium diffusion in stoichiometric UO_2, Catlow [39] reported a value of 4.8 eV, which is much higher than oxygen diffusion. Computational work by Cooper et al. [40] found that metastable clusters in UO_2 generate alternative diffusion pathways to that observed for a stable cluster configuration. These metastable clusters were shown to have lower migration enthalpies than the more stable clusters, and the cluster stability was dependant on the location of the oxygen and uranium vacancies in the UO_2 cell. The lowest migration enthalpy for U^{4+} ions via a vacancy mechanism calculated as 6.41 eV. Experimental work by Sabioni et al.

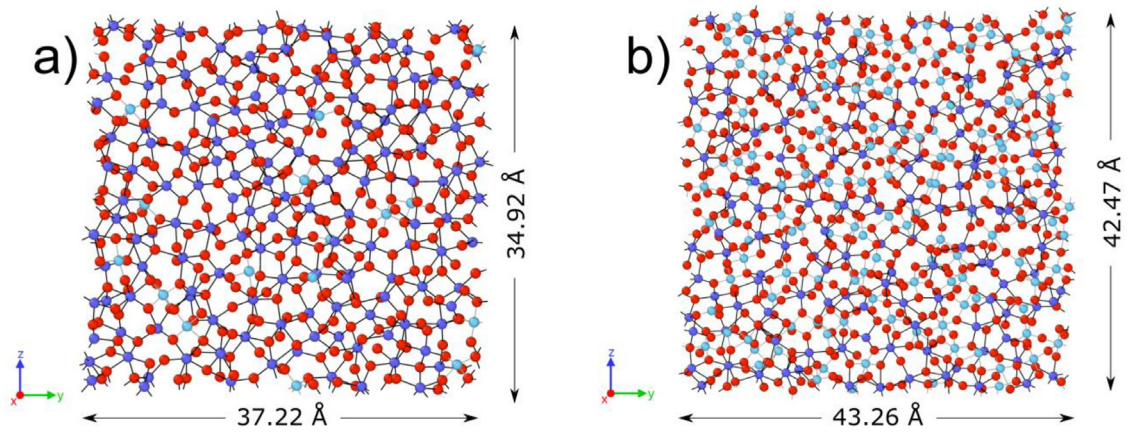

Fig. 6. 5 Å slice through a) 10 at.%, and b) 50 at.% amorphous Cr doped UO2 at 300 K, where oxygen = red, uranium = purple, chromium = blue, U-O bonds = black, Cr-O bonds = grey.

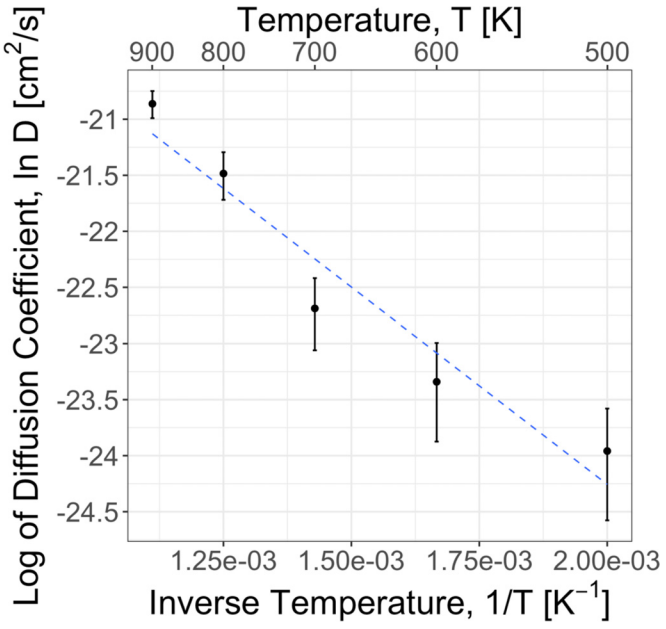

Fig. 7. Arrhenius plots for oxygen diffusion in amorphous undoped UO_2.

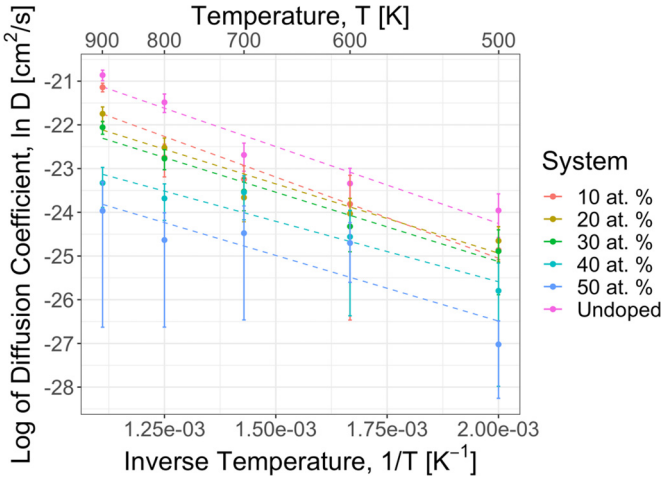

Fig. 8. Arrhenius plot for oxygen diffusion in Cr doped amorphous UO_2 systems.

Table 6
Diffusion data for oxygen diffusion in amorphous undoped and Cr doped systems.

Cr Concentration [at.%]	Activation Energy, E_A [eV]	Pre-exponential Factor, D_o [cm^2/s]
0	0.30 ± 0.05	3.32×10^{-8} $+ 4.28 \times 10^{-8}$ $- 1.87 \times 10^{-8}$
10	0.32 ± 0.06	2.22×10^{-8} $+ 4.28 \times 10^{-8}$ $- 1.46 \times 10^{-8}$
20	0.27 ± 0.05	8.38×10^{-9} $+ 1.25 \times 10^{-8}$ $- 5.01 \times 10^{-9}$
30	0.27 ± 0.03	6.98×10^{-9} $+ 5.70 \times 10^{-9}$ $- 3.14 \times 10^{-9}$
40	0.24 ± 0.04	1.94×10^{-9} $+ 2.07 \times 10^{-9}$ $- 1.00 \times 10^{-9}$
50	0.26 ± 0.08	1.27×10^{-9} $+ 3.65 \times 10^{-9}$ $- 9.40 \times 10^{-10}$

[41] found that the activation energy for uranium self-diffusion in stoichiometric UO_2 was 4.4 eV, reported as being much lower than theoretical work by Jackson et al. [42] on stoichiometric UO_2 at the temperature range considered (1498 – 1697 °C). Uranium self-diffusion has also been reported to be 4.55 eV in computational work conducted by Andersson et al. [43], on their works analysing Xe and U diffusion in UO_2. Often, high temperature analyses for uranium and oxygen ions have been conducted. The low temperatures used in this work limit the accurate prediction of the uranium diffusion (and chromium in the doped structures) and therefore they have not been reported but may be considered in future studies using accelerated dynamics methods.

Oxygen diffusion in doped amorphous UO_2 was computed successfully. Fig. 8 shows the Arrhenius plot for oxygen diffusion. With increasing concentration of Cr, the diffusion of oxygen ions decreases. This relates well with the use of additives in UO_2 fuel, to retard fission product diffusion to the grain boundaries [1,2,12]. Table 6 includes the activation energies and pre-exponential factors for oxygen diffusion in both undoped and doped UO_2 systems.

The activation energies for oxygen diffusion were relatively similar between all concentrations, ranging between 0.24 – 0.32 eV. When comparing activation energies to the Arrhenius plot (Fig. 8), it is expected that the activation energy of doped systems should increase with increasing Cr concentration, due to reduced diffusivity at higher concentrations. However, this is not observed. This could be within error, due to the larger error values observed at higher concentrations.

It is observed that in some cases increasing dopant concentration in crystalline oxides allows fast diffusion via a vacancy mech-

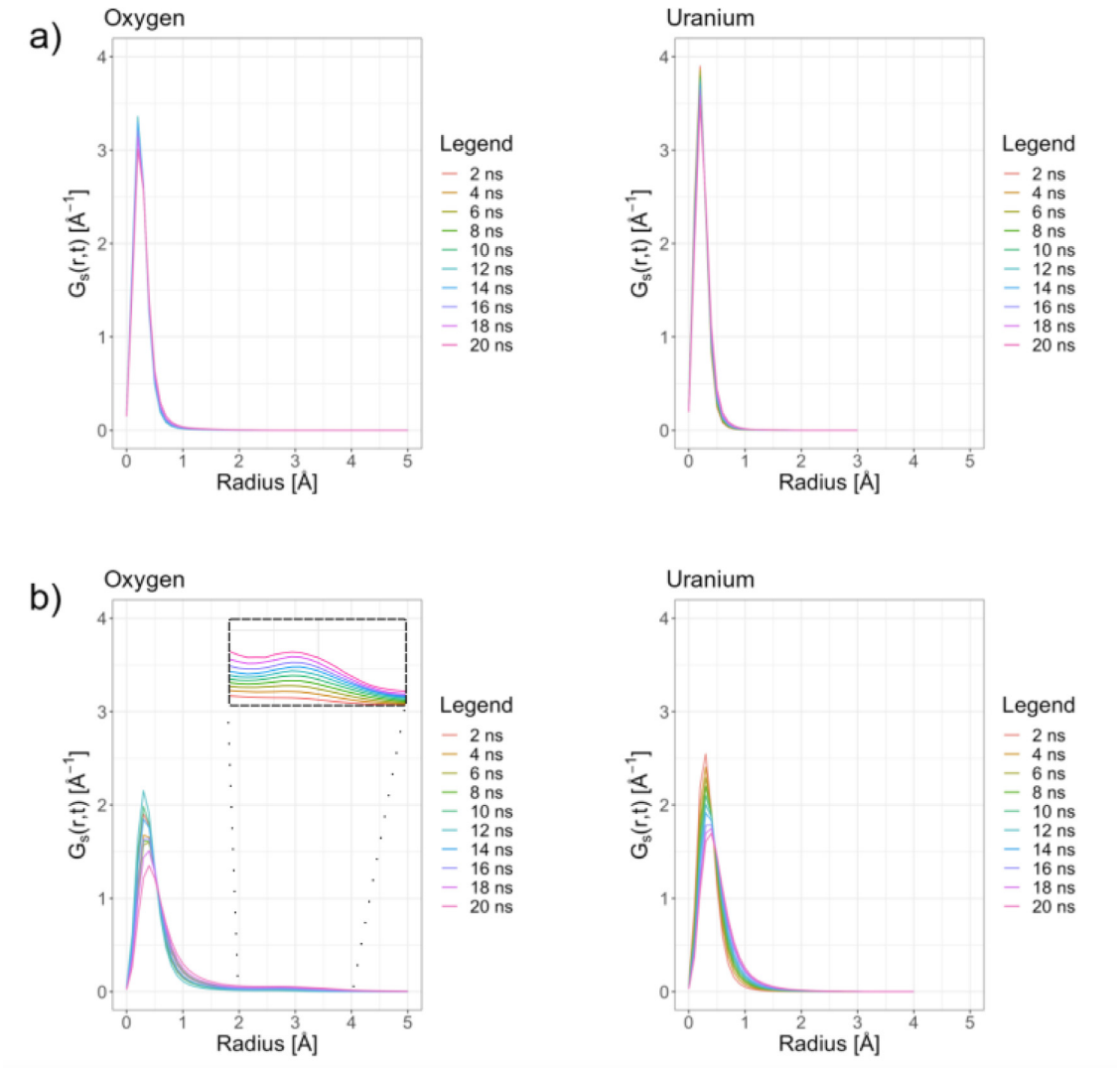

Fig. 9. Van Hove auto-correlation functions for oxygen and uranium diffusion at a) 500 K, and b) 900 K, in undoped amorphous UO2.

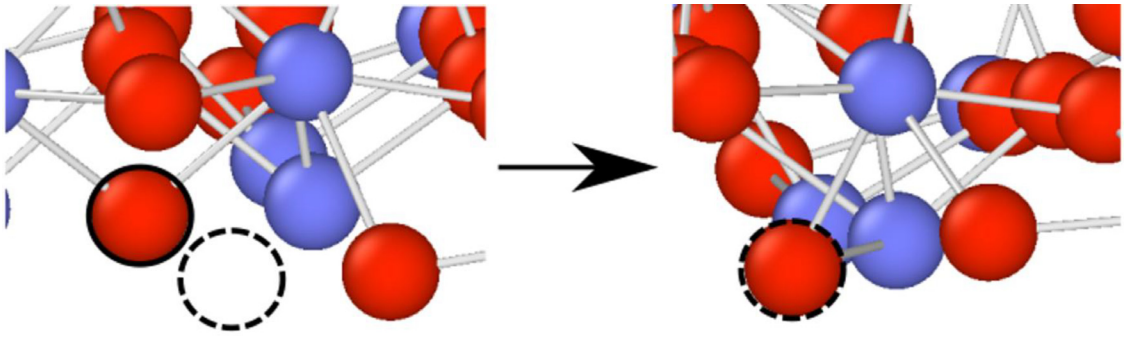

Fig. 10. Diffusion mechanism in 10 at.% Cr doped UO_2 at 900 K, where oxygen=red, uranium=purple, U-O bonds=grey. The solid line indicates the original position of the oxygen ion, and the dashed line indicates the final position of the oxygen ion.

anism, due to the increased number of oxygen vacancies present in the system (e.g. soluble yttria in zirconia [44]). The definition of a vacancy in an amorphous system is more complicated, and as no lattice structure exists, removal of oxygen is more appropriately characterised as a reduction in coordination [1]. The change in coordination environment in the system may cause the observed dependence of diffusion on dopant ions compared to the undoped system, with dopants having other roles in amorphous systems such as stabilizing the disordered structure.

The pre-exponential factors for oxygen diffusion range between 10^{-8} – 10^{-9} cm^2/s. Lower values were obtained at higher doping concentrations, indicating that fewer diffusion events are present. This relates well with the lower activation energy, indicating that oxygen ions are more readily moved from their position in the

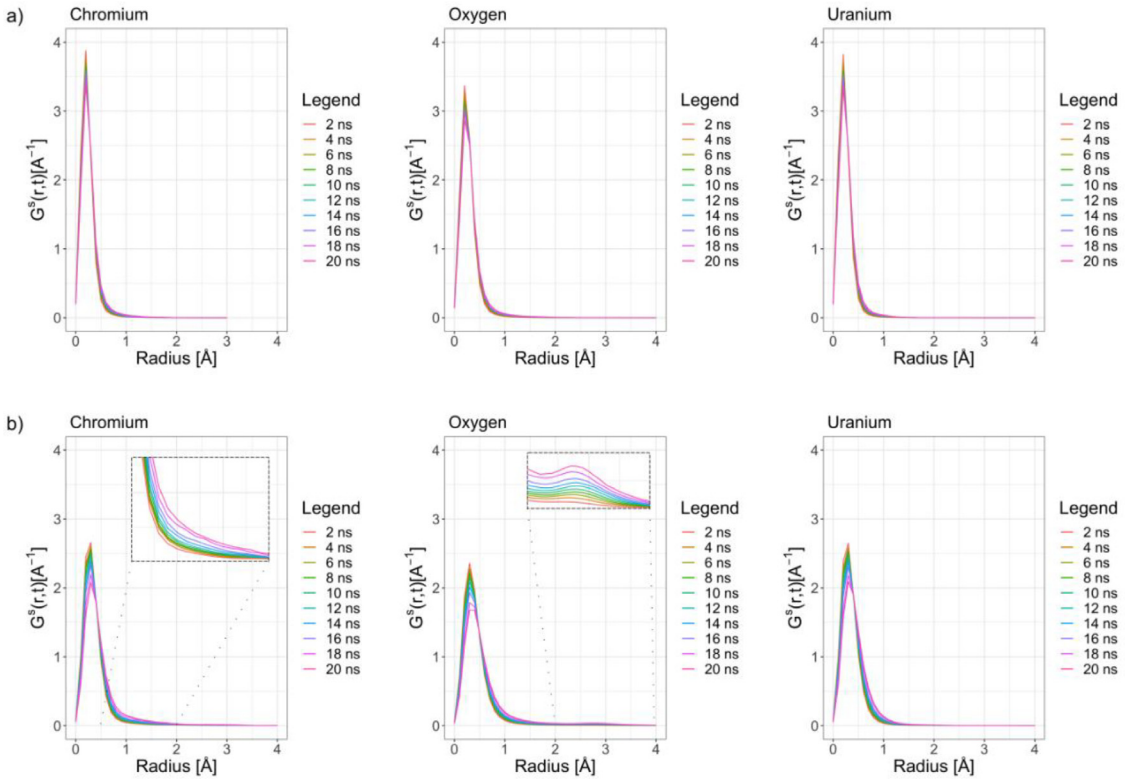

Fig. 11. Van Hove auto-correlation function plots for oxygen, uranium, and chromium diffusion in 10 at.% Cr doped amorphous UO_2 at a) 500 K, and b) 900 K.

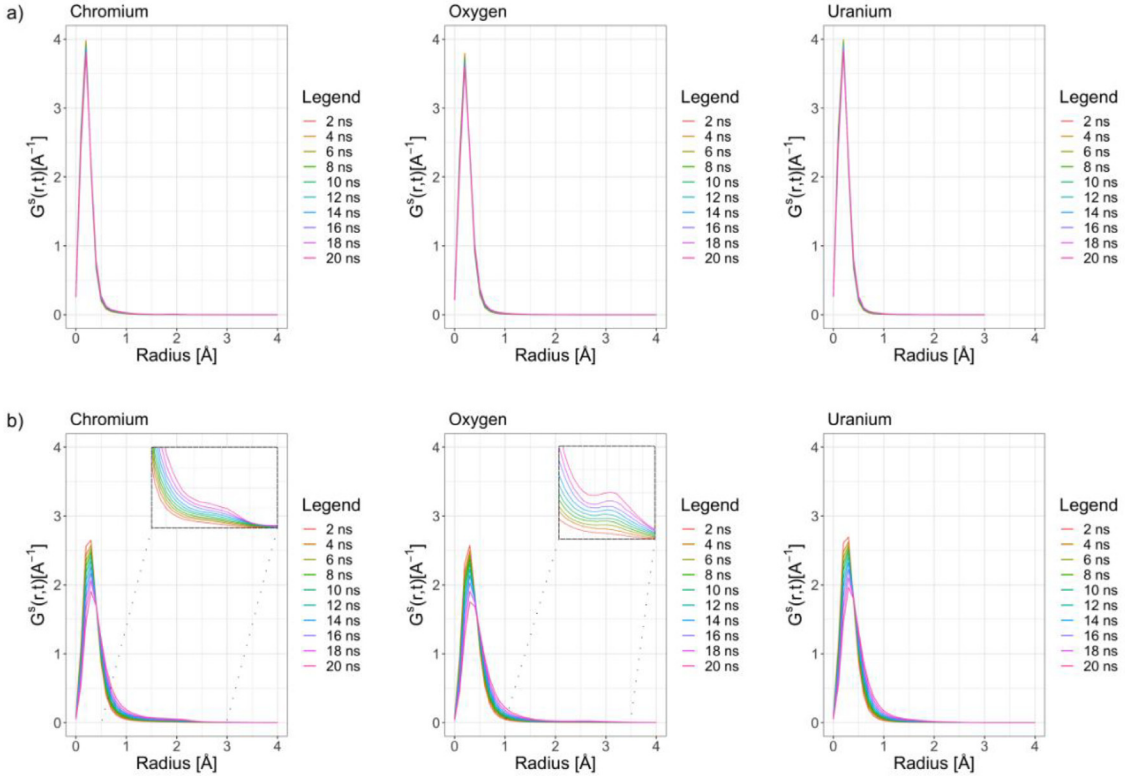

Fig. 12. Van Hove auto-correlation function plots for oxygen, uranium, and chromium diffusion in 50 at.% Cr doped amorphous UO_2 at a) 500 K, and b) 900 K.

undoped amorphous network compared to the doped amorphous system.

Van Hove auto-correlation functions are shown in Fig. 9 for oxygen and uranium diffusion in undoped UO_2 systems. Both ions experience a broadening of peaks at higher temperatures, indicative of diffusion events at higher temperatures. A second peak begins to emerge at approximately 3 Å at 900 K when considering oxygen diffusion, which is indicative of a hop-like mechanism of diffusion, like that observed in undoped amorphous ZrO_2 [32]. No peak is observed for the uranium plot at 900 K, indicative of little or no hop-like diffusion events.

Van Hove auto-correlation functions for oxygen, uranium, and chromium diffusion in 10 at.% and 50 at.% Cr doped amorphous UO_2 at 500 K and 900 K was also analysed, as shown in Figures 11 and 12. At both concentrations and at both temperatures analysed, oxygen and uranium ions have similar Van Hove autocorrelation function plots to the undoped counterpart, A secondary peak emerges in the oxygen plot at approximately 2.6 Å, indicative of a hop-like diffusion mechanism, as observed in the undoped system.

Further analysis of the diffusion mechanism was conducted using the OVITO [45] software. Trajectories of oxygen diffusion were analysed, to which a rearrangement of ions was observed to accommodate diffusion events. This analysis was also conducted for the undoped system, to which both diffusion mechanisms are identical. Fig. 10 shows the mechanism for diffusion observed in the Cr doped UO_2 systems. Future analysis of smaller cells would be beneficial in understanding the diffusion mechanism presented here. Impacts of undercoordinated cations in mediating anion diffusion would be analysed further to observe whether an orientation effect exists, even in amorphous undoped and doped UO_2 systems.

The Van Hove plots for Cr ions highlights that more diffusion events are observed in comparison to U ions, due to the peak broadening observed up until 2 Å. This relates well with experimental and theoretical works showing that Cr ions segregate towards grain boundaries and more favourable areas in the fuel. Further work will analyse the potential impacts of such segregation on fuel properties. [2]

4. Conclusions

Undoped and Cr doped amorphous UO_2 systems have been simulated successfully using classical molecular dynamics. The amorphous networks of the structures have been observed successfully, retaining a similar coordination environment of their crystalline counterparts. With increasing concentrations of Cr^{3+}, the amorphous UO_2 network is modified further, with network channels [46] clearly observed. The Cr^{3+} is acting as a network modifier, occupying the position in the tetrahedral UO_4 unit, in place of a uranium ion, impacting the coordination numbers of Cr – O and U – O pairs in the doped systems.

Diffusion of all constituent species in undoped and Cr doped amorphous UO_2 has been simulated successfully. Oxygen diffusion is fastest in undoped and doped amorphous systems. Oxygen diffusion is much faster in the undoped amorphous system compared to the undoped crystalline system, when comparing activation energies for oxygen diffusion with literature values. Diffusion of all species is observed in all Cr^{3+} doped amorphous systems. However, longer computation times are required to reliably predict diffusion accurately. Decreasing diffusivity of oxygen ions with increasing Cr concentration is observed, relating well with experimental works using dopants to retain fission gas products [1,2,12].

The mechanism for diffusion of oxygen in amorphous undoped and doped systems is similar to that of a hop-like mechanism observed in previous work assessing the behaviour of ionic solids [32]. The mechanism is mediated by a structural rearrangement of ions, to accommodate such diffusion events. Uranium ions are mostly immobile at both temperatures analysed. Chromium ions are however, mediated by a similar mechanism to that observed for oxygen ions, especially at 900 K temperatures.

Dopants are initially added to UO_2 fuel to obtain favourable properties such as larger grain sizes (40 – 55 μm [2]) and fission gas retention. However, with increasing concentrations of Cr, segregation of additions to favourable grain boundaries may increase. Increasing concentration of Cr in amorphous UO_2 cause the regions to become disordered and deviate from ordered grain boundaries, potentially stabilising the amorphous phases to higher temperatures. As Cr may stabilize the amorphous or disordered structure of the grain boundary (acting as a glass network modifier), it follows that the presence of Cr extends the temperature envelope in which enhanced diffusion along amorphous grain boundaries may be in effect, resulting in the larger grain sizes and higher pellet densities (10.67 g/cm^3 [2]) observed.

Further work will be conducted to analyse whether Cr additions truly stabilise amorphous structures that may be observed along grain boundary regions in Cr doped UO_2 fuel, stabilising these regions to higher temperatures. Further work on high burn up structures will also be analysed, to observe whether Cr poor sub grain boundaries also observe Cr segregation, as was observed in experimental work conducted by Fujino *et al.* [47] on 5 mol.% Mg and 5 mol.% Nb doped UO_2 pellets, where irradiation induced diffusion occurred, causing the Mg and Nb Dopants to segregate to sub grain boundary regions. This could also occur here, with Cr ions segregating to more favourable and undoped sub grain boundary regions. The effects of U^{5+} accommodation of Cr doped UO_2 will also be investigated. The accommodation of excess oxygen in UO_2 forming UO_{2+x} has been investigated in past works [48–50]. The excess oxygen can be accommodated by oxygen interstitial defects, where U^{4+} ions are oxidised to U^{5+} ions, or, or U^{4+} vacancies that are accommodated by oxidising four U^{4+} ions to form U^{5+} [48]. The solution mechanism for Cr changes into UO_{2+x} [28] however, to perform the assessments carried out in this work, one would need to consider, not only the movement of the atomic species (e.g. Cr, O and U), but also the migration of the charge from one uranium to another, possibly with the need of a charge transfer type empirical model [51]. Formation of $CrUO_4$ compounds will be analysed, where U has a formal charge of 5+. Formation of this compound will be analysed to observed whether it could potentially induce a liquid phase sintering regime within the fuel [52].

Declaration of competing interest

The authors declare the following financial interests/personal relationships which may be considered as potential competing interests:

Megan Owen reports financial support was provided by Westinghouse Electric Simon Middleburgh reports financial support was provided by Westinghouse Electric.

CRediT authorship contribution statement

Megan W. Owen: Conceptualization, Methodology, Formal analysis, Data curation, Writing – original draft. **Michael W.D. Cooper:** Conceptualization, Methodology, Formal analysis, Data curation, Writing – original draft. **Michael J.D. Rushton:** Conceptualization, Methodology, Software, Formal analysis, Writing – review & editing, Supervision. **Antoine Claisse:** Formal analysis, Writing – review & editing. **William E. Lee:** Formal analysis, Writing – review & editing. **Simon C. Middleburgh:** Conceptualization, Methodology, Formal analysis, Writing – review & editing, Supervision, Funding acquisition.

Data availability

Data will be made available on request.

Acknowledgements

This work has been carried out as part of a KESS 2 funded PhD project, with industrial sponsors being Westinghouse Springfields Ltd. This work has been performed within the framework of the international MUZIC (**M**echanistic **U**nderstanding of **Zi**rconium **C**orrosion) program. This work is associated with the MIDAS (**M**echanistic Understanding of **I**rradiation **D**amage in Fuel **As**semblies) forum. Knowledge Economy Skills Scholarships (KESS 2) is a pan-Wales higher level skills initiative led by Bangor University on behalf of the HE sector in Wales. It is part funded by the Welsh Government's European Social Fund (ESF) convergence programme for West Wales and the Valleys. SCM, WEL and MJDR are funded through the Sêr Cymru II programme by Welsh European Funding Office (WEFO) under the European Development Fund (ERDF). SCM is also supported through the EPSRC Enhanced Methodologies for Advanced Nuclear System Safety (eMEANSS – EP/T016329/1) project. MWDC was funded by the US Department of Energy, Office of Nuclear Energy, Nuclear energy Advance modeling and Simulation (NEAMS) program. This work was conducted as a part of the Sêr Cymru Strategic Partnership Acceleration Award – Strengthening links with US National Labs in Nuclear Energy Research, due to collaboration with Los Alamos National Laboratory. Computing resources were made available by HPC Wales and Supercomputing Wales.

References

[1] S.C. Middleburgh, et al., Structure and properties of amorphous uranium dioxide, Acta Mater. 202 (Jan. 2021) 366–375, doi:10.1016/j.actamat.2020.10.069.
[2] J. Arborelius, et al., Advanced doped UO_2 pellets in LWR applications, J. Nucl. Sci. Technol. 43 (9) (2006) 967–976, doi:10.1080/18811248.2006.9711184.
[3] P.v. Nerikar, et al., Grain boundaries in uranium dioxide: scanning electron microscopy experiments and atomistic simulations, J. Am. Ceramic Soc. 94 (6) (Jun. 2011) 1893–1900, doi:10.1111/j.1551-2916.2010.04295.x.
[4] E. Bourasseau, et al., Experimental and simulation study of grain boundaries in UO_2, J. Nucl. Mater. 517 (Apr. 2019) 286–295, doi:10.1016/j.jnucmat.2019.02.033.
[5] H. Kleykamp, The chemical state of fission products in oxide fuels, J. Nucl. Mater. 131 (1985) 221–246.
[6] M. Hong, et al., The role of charge and ionic radius on fission product segregation to a model UO_2 grain boundary, J. Appl. Phys. 113 (13) (Apr. 2013), doi:10.1063/1.4798347.
[7] P.R. Cantwell, et al., Grain boundary complexions, Acta Mater. 62 (1) (2014) 1–48, doi:10.1016/j.actamat.2013.07.037.
[8] P.v. Nerikar, et al., Segregation of xenon to dislocations and grain boundaries in uranium dioxide, Phys. Rev. B Condens. Matter. Mater. Phys. 84 (17) (Nov. 2011), doi:10.1103/PhysRevB.84.174105.
[9] P. Kegler, et al., Chromium doped UO_2-based ceramics: synthesis and characterization of model materials for modern nuclear fuels, Materials (Basel) 14 (20) (Oct. 2021), doi:10.3390/ma14206160.
[10] A.R. Symington, et al., Defect segregation facilitates oxygen transport at fluorite UO_2 grain boundaries, Philos. Trans. R. Soc. A 377 (2152) (Aug. 2019), doi:10.1098/rsta.2019.0026.
[11] G. Pastore, et al., Physics-based modelling of fission gas swelling and release in UO_2 applied to integral fuel rod analysis, Nucl. Eng. Des. 256 (2013) 75–86, doi:10.1016/j.nucengdes.2012.12.002.
[12] H. Assman, et al., Letter to the Editors: doping UO_2 with niobia - beneficial or not? J. Nucl. Mater. 98 (1981) 216–220.
[13] D.R. Costa, et al., Individual influence of Al_2O_3 and Nb_2O_5 on grain growth of UO_2 sintered pellets manufactured at INB, International Nuclear Atlantic Conference, 2013.
[14] J.C. Killeen, The effect of additives on the irradiation behaviour of UO_2, J. Nucl. Mater. 58 (1975) 39–46.
[15] N.R. Williams, et al., Atomistic investigation of the structure and transport properties of tilt grain boundaries of UO_2, J. Nucl. Mater. 458 (2015) 45–55, doi:10.1016/j.jnucmat.2014.11.120.
[16] Hj. Matzke, Diffusion in Doped UO_2, Nucl. Appl. 2 (2) (Apr. 1966) 131–137, doi:10.13182/nt66-a27493.
[17] A.C.S. Sabioni, et al., Letter to the Editors: effect of grain-boundaries on uranium and oxygen diffusion in polycrystalline UO_2, J. Nucl. Mater. 278 (2000) 364–369.
[18] T. Kubo, et al., Effects of gadolinium doping on electrical properties of UO_2 grain boundaries, J. Nucl. Sci. Technol. 30 (7) (1993) 664–672, doi:10.1080/18811248.1993.9734532.
[19] M.W.D. Cooper, et al., A many-body potential approach to modelling the thermomechanical properties of actinide oxides, J. Phys. Condensed Matter 26 (10) (Mar. 2014), doi:10.1088/0953-8984/26/10/105401.
[20] M.J.D. Rushton, "Potential-Pro-fit (pprofit)."
[21] J.D. Gale, GULP: a computer program for the symmetry-adapted simulation of solids, J. Chemical Soc. Farady Trans. 93 (1997) 629–637.
[22] A.H. Hill, et al., Crystallographic and magnetic studies of mesoporous eskolaite, Cr_2O_3, Microporous Mesoporous Mater. 130 (1–3) (May 2010) 280–286, doi:10.1016/j.micromeso.2009.11.021.
[23] H.L. Alberts, J.C.A. Boeyens, The elastic constants and distance dependence of the magnetic interactions of Cr_2O_3, J. Magn. Magn. Mater. 2 (1976) 327–333.
[24] J.A. Nelder, R. Mead, A simplex method for function minimization, Comput. J. 7 (1965) 308–313, doi:10.1093/comjnl/7.4.308.
[25] A.M. Dymshits, et al., Thermoelastic properties of chromium oxide Cr_2O_3 (eskolaite) at high pressures and temperatures, Phys. Chem. Miner. 43 (6) (Jun. 2016) 447–458, doi:10.1007/s00269-016-0808-7.
[26] H. Kudielka, Die thermisehe Ausdehnung tier isotypen Mischreihen-Endglieder Cr_2O_3 und a-Al_3O_2, ermittelt mit einer neuen, lichtstarken Seemann - Bohlin-Kammer, Montasjefte fur Chemie (1972) 72–80.
[27] P. Hirel, Atomsk: a tool for manipulating and converting atomic data files, Comput. Phys. Commun. 197 (Dec. 2015) 212–219, doi:10.1016/j.cpc.2015.07.012.
[28] S.C. Middleburgh, et al., Solution of trivalent cations into uranium dioxide, J. Nucl. Mater. 420 (1–3) (Jan. 2012) 258–261, doi:10.1016/j.jnucmat.2011.10.006.
[29] A. Leenaers, et al., On the solubility of chromium sesquioxide in uranium dioxide fuel, J. Nucl. Mater. 317 (1) (Apr. 2003) 62–68, doi:10.1016/S0022-3115(02)01693-8.
[30] S. Plimpton, Fast parallel algorithms for short-range molecular dynamics, J. Comput. Phys. 117 (1995) 1–19.
[31] H.J. Matzke, et al., The crystallization of amorphous UO_2, Thin Solid Films 22 (1974) 75–82.
[32] M.W. Owen, et al., Diffusion in doped and undoped amorphous zirconia, J. Nucl. Mater. 555 (Nov. 2021), doi:10.1016/j.jnucmat.2021.153108.
[33] P. Hopkins, et al., The van Hove distribution function for Brownian hard spheres: dynamical test particle theory and computer simulations for bulk dynamics, J. Chem. Phys. 133 (22) (Dec. 2010), doi:10.1063/1.3511719.
[34] M.W.D. Cooper, et al., Thermophysical and anion diffusion properties of (Ux,Th1-x)O_2, Proc. R. Soc. A 470 (2171) (Nov. 2014), doi:10.1098/rspa.2014.0427.
[35] L. Desgranges, et al., Neutron diffraction study of the in situ oxidation of UO_2, Inorg. Chem. 48 (16) (Aug. 2009) 7585–7592, doi:10.1021/ic9000889.
[36] J.J. Carey, M. Nolan, Influence of trivalent doping on point and Frenkel defect formation in bulk chromium (III) oxide, Solid State Ion 307 (Sep. 2017) 51–64, doi:10.1016/j.ssi.2017.04.016.
[37] P. Li, et al., Effect of dopants on zirconia stabilization-An X-ray absorption study: I, trivalent dopants, J. Am. Ceramic Soc. 77 (1) (1994) 118–128.
[38] G.E. Murch, et al., Oxygen Diffusion in UO_2, ThO_2 and PuO_2, J. Chem. Soc., Faraday Trans. 2 83 (1987) 1157–1169.
[39] C.R.A. Catlow, Point defect and electronic properties of uranium dioxide, R. Soc. Lond. A. 353 (1977) 533–561.
[40] M.W.D. Cooper, et al., Vacancy mediated cation migration in uranium dioxide: the influence of cluster configuration, Solid State Ion 266 (Nov. 2014) 68–72, doi:10.1016/j.ssi.2014.08.010.
[41] A.C.S. Sabioni, et al., First study of uranium self-diffusion in UO_2 by SIMS, J. Nucl. Mater. 257 (1998) 180–184.
[42] R.A. Jackson, et al., The calculation of defect parameters in UO_2, Philos. Mag. A 53 (1) (1986) 27–50, doi:10.1080/01418618608242805.
[43] D.A. Andersson, et al., Multiscale simulation of xenon diffusion and grain boundary segregation in UO_2, J. Nucl. Mater. 462 (Jul. 2015) 15–25, doi:10.1016/j.jnucmat.2015.03.019.
[44] M. Kilo, et al., Oxygen diffusion in yttria stabilised zirconia - experimental results and molecular dynamics calculations,", Phys. Chem. Chem. Phys. 5 (11) (2003) 2219–2224 *Jun*, doi:10.1039/b300151m.
[45] A. Stukowski, Visualization and analysis of atomistic simulation data with OVITO-the open visualization tool, Model Simul. Mat. Sci. Eng. 18 (1) (2010), doi:10.1088/0965-0393/18/1/015012.
[46] G.N. Greaves, EXAFS and structure of glass, J. Non Cryst. Solids 71 (1985) 203–217.
[47] T. Fujino, et al., Post-irradiation examination of high burnup Mg doped UO_2 in comparison with undoped UO_2, Mg±Nb doped UO_2 and Ti doped UO_2, J. Nucl. Mater. 297 (2001) 176–205.
[48] A. Taskinen, H. Kullberg, Oxygen chemical diffusion coefficient in Hyperstoichiometric uranium dioxide, J. Nucl. Mater. 83 (1979) 333–334.
[49] J.W. Wang, et al., Average structure and local configuration of excess oxygen in UO_{2+x}, Sci. Rep. 4 (Mar. 2014), doi:10.1038/srep04216.
[50] B.T.M. Willis, The defect structure of hyper-stoichiometric uranium dioxide, Acta Cryst 34 (1978) 88–90.
[51] Y. Li, et al., A charge-optimized many-body potential for the U-UO_2-O_2 system, J. Phys. Condensed Matter 25 (50) (Dec. 2013), doi:10.1088/0953-8984/25/50/505401.
[52] M.W.D. Cooper, et al., Formation of (Cr, Al)UO_4 from doped UO_2 and its influence on partition of soluble fission products, J. Nucl. Mater. 443 (1–3) (2013) 236–241, doi:10.1016/j.jnucmat.2013.07.038.